

Chiral patterns arising from electrostatic growth models

Ilya M. Sandler^{1,2}, Geoffrey S. Canright^{1,2}, Hongjun Gao^{3,2}, Shijin Pang³, Zengquan Xue⁴, and Zhenyu Zhang^{2,1}

¹*Department of Physics and Astronomy, University of Tennessee,
Knoxville, Tennessee 37996-1200, USA*

²*Solid State Division, Oak Ridge National Laboratory,
Oak Ridge, Tennessee 37831-6032, USA*

³*Beijing Laboratory of Vacuum Physics, Chinese Academy of Sciences,
Beijing 100080, PRC*

⁴*Department of Electronics, Peking University, Beijing 100871, China*

Recently, unusual and strikingly beautiful seahorse-like growth patterns have been observed under conditions of quasi-two-dimensional growth. These ‘S’-shaped patterns strongly break two-dimensional inversion symmetry; however such broken symmetry occurs only at the level of overall morphology, as the clusters are formed from achiral molecules with an achiral unit cell. Here we describe a mechanism which gives rise to chiral growth morphologies without invoking microscopic chirality. This mechanism involves trapped electrostatic charge on the growing cluster, and the enhancement of growth in regions of large electric field. We illustrate the mechanism with a tree growth model, with a continuum model for the motion of the one-dimensional boundary, and with microscopic Monte Carlo simulations. Our most dramatic results are found using the continuum model, which strongly exhibits spontaneous chiral symmetry breaking, and in particular finned ‘S’ shapes like those seen in the experiments.

PACS numbers: 47.54.+r,61.43.Hv,68.70.+w

I. INTRODUCTION

Growth phenomena are known for the complexity and beauty of the patterns they can lead to [1]. Most of this complexity results from different kinds of instabilities associated with growth, such as the Mullins-Sekerka instability of growth fronts [2], or fingering instability [3–5]. The presence of instabilities implies that a tiny microscopic noise can result in macroscopic changes of shape, and hence lead to a variety of shapes. (For instance, the formation of snowflakes, a growth phenomenon familiar to everyone, produces hundreds of different shapes [6]). However, despite the variety of shapes, the vast majority of growth patterns preserve left-right symmetry; in other words, essentially all of the known growth patterns are *achiral*. One well-known and historic exception is the appearance of hemihedral faces on crystals, yielding faceted forms which are not invariant under inversion [7]. In the mid-19th century, such faces were identified in molecular crystals of sodium ammonium tartrate by Pasteur, and the broken chiral symmetry was ascribed by him to the microscopic chirality of the constituent molecules.

In this work we concentrate on two-dimensional (or quasi-two-dimensional) growth forms. For two-dimensional forms the relevant inversion operator is $x \rightarrow -x$ or $y \rightarrow -y$, but not both; we will call such an operation “2D inversion”, and forms distinguishable from their 2D inverse “2D chiral”. (Also, since we concentrate entirely on 2D henceforth, we will sometimes shorten these terms by omitting the leading “2D” qualifier.) 2D chiral growth forms are not common [8]. In those rare cases where chiral growth patterns do appear [9,10], the inversion symmetry is already broken at the microscopic level. An example is the formation of spiral crystals [9] during the compression of a phospholipid monolayer on a water-air interface. In this case the individual phospholipid molecules possess a 3D chirality. Each molecule also has a preferential orientation (hydrophilic head down) with respect to the water-air interface. This consistent orientation then gives a monolayer with *two-dimensional* inversion symmetry already broken [11] at the microscopic level—assuming only that the molecules themselves have a predominance of a single enantiomer. And in fact, for spiral crystals to appear, one needs to have a monolayer consisting predominantly of a single enantiomer. The handedness of the crystals depends directly on the handedness of the dominant enantiomer, and no chirality appears for racemic monolayers [9]. While there are several competing explanations of how the microscopic chirality leads to the macroscopic chirality [12,13], it is nevertheless clear that the latter occurs only because of the former. Similarly, in another chiral growth example—the formation of chiral bacterial colonies [10]—the individual particles (bacteria) also have a three-dimensional chirality (of a single ‘sign’) which then manifests itself as a 2D chirality when coupled with a 2D substrate. The bacterial aggregates are observed to be (2D) chiral, and always with the same handedness [10]. Thus, in each of these cases, it is clear that the macroscopic 2D chirality of the aggregates results from a microscopic 3D chirality of the elementary building blocks.

Recently, a novel and very beautiful type of growth pattern has been reported [14,15]. A typical pattern strikingly resembles a seahorse (in the form of an ‘S’ shape, with ‘fins’ on the outer curved edges), and so has a strongly broken 2D inversion symmetry. The patterns were discovered during growth studies of fullerene-tetracyanoquinodimethane (C₆₀-TCNQ) thin films. Sub-

arXiv:cond-mat/9809198v1 14 Sep 1998

sequently, very similar patterns were obtained using TCNQ only [16]. The broken symmetry is one of the most striking aspects of the patterns, as well as one of the principal mysteries connected with them. The mystery arises because—in contrast to the two cases mentioned above—in these experiments there is *no* microscopic symmetry breaking: TCNQ molecules are themselves inversion symmetric [17]. Furthermore, even though the ‘seahorse’ aggregates are polycrystalline [14], one can probably rule out symmetry breaking at the level of the unit cell, since TCNQ crystals are also achiral [17,18].

It is however important to note that both left- and right-handed patterns appear in approximately equal numbers [16]. Thus, on average, the experiment does not break inversion symmetry; instead the symmetry is broken *spontaneously*, for each island, during the growth. That is, the “seahorse” growth experiments represent an almost unique case of spontaneous 2D chiral symmetry breaking during quasi-two-dimensional growth.

We say ‘almost’ unique because we are aware of only one other growth phenomenon exhibiting such spontaneous symmetry breaking, namely, phyllotaxis: the pattern of leaves, buds, scales, etc in growing plants [19]. As demonstrated by Douady and Couder [20], this phenomenon can be understood cleanly in two dimensions; and furthermore, the resulting spiral growth patterns are clearly chiral, and the symmetry breaking is clearly spontaneous [19,20]. Outside of this one example from botany, however, we know of no example of two-dimensional growth—experimental or theoretical—in which the resulting growth patterns spontaneously break 2D inversion symmetry.

In this work we construct a growth model which does yield such spontaneous symmetry breaking. More precisely, we consider a set of models, all embodying the same ideas. These ideas involve a novel form of long-ranged branch competition and growth, arising from electrostatic effects. We have found that such a mechanism can lead to growth forms which spontaneously break two-dimensional inversion symmetry.

The growth models which we will consider share several important properties. These properties are simple, and can be formulated independently of the nature of the underlying physical processes. The physical picture which we consider involves the following elements: (i) branching, that is, every growing branch should eventually give rise to new branches; (ii) strong branch competition—in fact, the competition has to be so strong, that only 2 main branches “survive”; (iii) long range branch repulsion: the two branches need to “feel” one another and curve away from each other.

Branching is a very common property in growth phenomena [1]. Branch competition is also very common. It is usually caused by screening—that is, by the competition between growing branches for incoming particles. But competition due to screening alone is not strong enough to lead to two-armed shapes. For instance, the diffusion-limited aggregation (DLA) model leads to clus-

ters having 4 or more branches [21–25]. Competition for incoming particles may also cause some branch repulsion. But this effect is obviously very short-ranged (a branch “feels” only its neighbors). Thus in order to achieve (i)–(iii), one needs to introduce a long-ranged interaction into the system. As will be discussed later in section III A, electrostatic forces may play an important role in the formation of the seahorse patterns. Hence, in our models, the long range interaction between branches is also of electrostatic origin.

We will start with a very simple deterministic “tree” growth model which has properties (i)–(iii) by construction, and show that this model prefers chiral rather than symmetric shapes. We will then consider a more realistic quasi-equilibrium continuum model, in which properties (ii)–(iii) arise naturally due to electrostatic interactions. This model yields two-armed, finned, S-shaped forms for a range of growth parameters, for essentially the same physical reasons as does the tree model. We also report some preliminary studies involving the same physical ideas but using a microscopic Monte-Carlo approach. These modeling efforts are inspired by the puzzling and remarkable experimental patterns; and they yield qualitatively similar growth forms. It is also encouraging that further growth experiments involving a static in-plane electric field (which we discuss briefly below, and in detail in another paper [16]) have provided support for our ideas.

II. CHARGED TREES

In this section we demonstrate, using a simple and highly schematic model, how long-ranged branch repulsion and competition may cause chiral symmetry breaking. We will formulate a simple growth model where such branch repulsion and competition are present by construction, and show that chiral ‘S’ shapes are preferred energetically over symmetric shapes.

A charged tree model is constructed as follows (Fig. 1). A tree starts as a single charged rod. The ends of this rod are considered to be “alive”. Then each alive branch emits two branches: one branch of length l_0 and the other of length l_1 . Both new branches grow at a predefined angle θ . All three quantities— l_0 , l_1 , and θ —are the same for opposite ends, and do not vary during the growth. When $l_0 \neq l_1$, there are 4 possible combinations of growth on every step; among these, the model chooses the tree with the lowest electrostatic energy. Then the longer of the newly added branches become new “alive” branches, the shorter ones “die”, and the process is repeated again. If two (or more) configurations have the same energy then the selection is done randomly. The first 2 steps of growth are shown in Fig. 1.

To complete this model we need to specify how we will compute the electrostatic energy, as the energy of a 1D charged rod diverges. The most obvious way to deal with

this problem is to assign some small (but finite) width w to the branches, with this width satisfying $w \ll l_0, l_1$. This allows us to work with 2D, rather than 1D, charge density. To compute the electrostatic energy of the tree, we further break the branches into smaller (linear) pieces. The i th piece has the length l_i , and the linear charge density λ_i , which is in an obvious way related to 2D charge density $\sigma_i = \lambda_i/w$.

We will consider 2 possible charge distributions: 1) a conducting charge distribution $U_i = \text{const}$, where U_i is the potential at the center of the i -th piece; 2) a uniform charge distribution $\sigma_i = \text{const}$. In both cases the total charge of the system will be normalized by the requirement that the average linear charge density be equal to unity, that is

$$\bar{\lambda} = \sum_i \lambda_i l_i / L = 1 \quad (2.1)$$

where $L = \sum_i l_i$ is the total length of the structure.

To find the charge densities for each piece we construct a set of linear algebraic equations

$$\sum_{j=0}^{N-1} U_{ij} \lambda_j = 1 \quad (2.2)$$

where $i = 0, \dots, N-1$, and U_{ij} is the electrostatic potential which would be induced at the center of the i -th piece by the j -th piece if the latter had a *unit* charge density. Clearly the solution $\{\lambda_i\}$ of Eq. (2.2) meets the requirement $U_i = \text{const}$ (the constant was set to 1); this solution can then be easily rescaled to meet the normalization condition (2.1).

Using elementary electrostatics, one can show that the constants U_{ij} are given by

$$U_{ii} = 2 \ln(5.44w/l_i) \quad (2.3)$$

and for $i \neq j$

$$U_{ij} = \ln \frac{\sqrt{(l_j/2 - x_i)^2 + y_i^2} + (l_j/2 - x_i)}{\sqrt{(l_j/2 + x_i)^2 + y_i^2} - (l_j/2 + x_i)} \quad (2.4)$$

where l_j is the length of j -th piece, x_i, y_i are the coordinates of the center of the i -th piece (the origin is assumed to be at the center of the j -th piece, and the x -axis directed along the j -th piece).

The growth of such trees was studied numerically, and all trees grown according to these rules demonstrate some chirality. One of the typical S-like shapes is shown in Fig. 2.

Why does the tree prefer to break the left/right symmetry? To answer this question, we note that, by introducing the repulsive electrostatic interaction, we effectively made the tree keep its branches as far away from each other as possible. This observation alone accounts for the fact that the tree “chose” the ‘S’ shape on the

first split. However, during subsequent splits the result is determined by the interaction between *all* branches, and the outcome depends crucially on how the charge is distributed over the tree: the more charge is concentrated on the small “dead” branches, the stronger is the symmetry breaking (i.e. the higher is the achievable curvature of the main arms). We can illustrate this point by considering the case of a uniform charge distribution $\lambda_i = \text{const}$. In this case the potential energy of a tree is given by

$$U_u = \frac{1}{2} \sum_{i,j} U_{ij} \lambda_j \lambda_i l_i = \frac{\lambda^2}{2} \sum_{i,j} U_{ij} l_i \quad (2.5)$$

We have grown a number of trees using the above rules, but with the assumption of a uniform charge distribution. The resulting trees have a much more weakly broken symmetry, which comes primarily from the symmetry breaking at the first branching; and they are not S-shaped.

This result is consistent with the idea that a higher charge density on the external “dead” branches (which results for instance from the conducting charge distribution) enhances the overall chirality of the cluster. We will return to the question of how the charge redistribution influences which branches survive or die in the next section.

We also note that one can construct a non-deterministic charged tree growth model, where the growth rates themselves are determined by the electrostatic interaction between branches. This non-deterministic growth model also leads to a spontaneous chiral symmetry breaking [26].

III. THE CONTINUUM MODEL

A. Construction of the Model

In this section we will consider a more realistic growth model, in which strong branch competition and survival of only 2 main arms occur naturally (for some range of parameters). That is, for the model we now describe, properties (ii)–(iii) (strong branch competition and repulsion) arise as a result of the *dynamics* of growth. In common with the tree models described above, a crucial ingredient is the presence of a long-ranged electrostatic interaction.

First we will consider in more detail what actually happens in the “seahorse” experiments [14,15]. In these experiments layers of TCNQ are deposited using the ionized cluster beam (ICB) deposition [27,28] method. With this method the TCNQ molecules are ionized and then accelerated towards the substrate, where they arrive with high kinetic energy (and thus high mobility) and therefore can diffuse along the substrate and form growing clusters. A small fraction α of the diffusing particles (estimated [16] to be typically $\sim 10\%$) are charged (all

of the same sign). Thus the growing islands will also carry some (time-dependent) charge. The magnitude and time dependence of this charge are not known; it depends on many complicating factors, including the repulsion of the charged, diffusing particles by the charge on the island; leakage to the substrate, both from the diffusing charged walkers and from the charged aggregate; and the “rain” of charged particles directly on the growing islands. We will treat this time-dependent charge $Q(t)$ in an extremely simple way below; our motivation is to explore the kinds of effects that electrostatic charge may have on growth processes.

The field of the island, in contrast with the field of walkers, is not random, and therefore will play the dominant role in how the particles (walkers) diffuse. Hence in our work we neglect the random field of the walkers. We assume that neutral walkers have a non-zero polarizability; hence the diffusive motion of both charged and neutral walkers is affected by the electrostatic field of the aggregates. To consider the simplest case, we will neglect any possible cluster-cluster interactions and consider only the growth of an isolated island.

An obvious approach to this problem would be a Monte Carlo (MC) simulation. However, a simple estimate of the number of particles in seahorse clusters in the experiments gives 10^6 – 10^7 particles. A direct microscopic Monte-Carlo simulation for a problem of this size is very hard, if not impossible. We have performed some limited MC studies (involving much smaller particle numbers, ie $N \sim 10^3$), which we will describe briefly in section IV. Here we will consider an alternative approach, in which, instead of tracing the motion of individual particles, we will compute local growth rates for the cluster boundary, which we treat as a continuous 1D curve. We will obtain equations for the motion of this 1D curve, and study the kinds of growth that result.

First, let us consider a growing island surrounded by diffusing walkers. If a walker hits the island, then with some probability p_s (“sticking” probability) it (the walker) becomes a part of the island. Then the local growth rate is

$$\vec{G}(x, y, t) = \frac{d\vec{h}(x, y)}{dt} = \hat{n}(x, y)\delta_m^2 \frac{d^2 N_{hits}(x, y)}{dt dl} p_s \quad (3.1)$$

where $d\vec{h}(x, y)$ is the displacement of the given boundary point (x, y) during the time dt , $\hat{n}(x, y)$ is the unit vector normal to the boundary, δ_m is a typical intermolecular distance in the growing cluster (thus, δ_m^2 is the area occupied by a single molecule), and $d^2 N_{hits}(x, y)/(dt dl)$ is the number of hits per unit boundary length per unit time. We then take

$$\frac{d^2 N_{hits}(x, y)}{dt dl} = \alpha_{hits} N(x, y) v_T \quad (3.2)$$

where $N(x, y)$ is the walker concentration near the point (x, y) on the boundary, v_T is an average thermal velocity of the walkers, and α_{hits} is a numerical factor of order of

unity. Thus, we can rewrite the equation for local growth rates as

$$\vec{G}(x, y, t) = \frac{d\vec{h}(x, y)}{dt} = \hat{n}(x, y) G_T p_s N(x, y) \quad (3.3)$$

where $G_T = \alpha_{hits} v_T \delta_m^2$ is a constant which depends only on the temperature.

Here we will assume that the growth is slow enough to be considered as a quasi-equilibrium process (which is the case when $p_s \ll 1$). Our motivations for this assumption are twofold: first, it is physically motivated, in that the sticking probability may indeed be very small, due to the high kinetic energy of the walkers in an ICB experiment; and second, it makes the problem tractable, giving a simple form for $N(x, y)$ which enables us to concentrate on the motion of the boundary. Given this assumption, then, the concentration of walkers is given by a quasi-equilibrium Boltzmann distribution: $N(x, y, t) = N^{(0)} \exp[-U(x, y, t)/kT]$ where $U(x, y)$ is the potential energy of a walker at the point (x, y) , $N^{(0)}$ is the concentration far away from the cluster, and k is Boltzmann’s constant.

In our case there are 2 different kinds of particles present in the system: charged and neutral walkers, each kind having a different concentration and a different potential energy function. The overall growth rate is given by

$$dh(x, y, t)/dt = dh_n/dt + dh_c/dt \quad (3.4)$$

where the subscript n denotes neutral walkers, and the subscript c charged walkers. The walker concentrations are given by

$$N_\beta(x, y, t) = N_\beta^{(0)} \exp[-U_\beta(x, y, t)/kT] \quad (3.5)$$

with $\beta = n$ or c and (as discussed above) $N_c^{(0)} \ll N_n^{(0)}$. The potential energy $U(x, y)$ is equal to $-\chi E^2/2$ for neutral walkers (of polarizability χ) in a field $E = |\vec{E}(x, y, t)|$, and $V(x, y, t)e$ for charged walkers.

Now we assume that the cluster is conducting. As with the quasiequilibrium assumption, our reasons are both computational and physical: the conducting cluster is rather straightforward to treat numerically (and even analytically in some special cases); but also, from our charged-tree studies, we expect that a conducting cluster will enhance the type of branch competition which we wish to study here. For a conducting cluster, U_c (and hence dh_c/dt) are each independent of position on the island. The applicability of this assumption to the seahorse experiments will be discussed below.

The model we have constructed thus far requires the computation of the electric field due to the charge on a two-dimensional growing cluster, which is in general of an irregular shape. This electric field is determined by the charge distribution $\sigma(x, y, t)$ on the island. However, $\vec{E}(x, y)$ diverges near the edge of any 2D charge distribution; hence, instead of using the field at the edge, we

will use the field at a small (molecular) distance from the edge. That is, instead of $\vec{E}(x, y, t) = \vec{E}(\vec{r}, t)$ we will use $\vec{E}(\vec{r} + \delta \cdot \hat{n}(x, y), t)$, where δ is the ‘sticking distance’—the distance at which a diffusing particle sticks to the cluster; we will assume $\delta \sim \delta_m$. The electric field is determined by the shape of the island, to within an overall scale factor given by Q , the net charge on the island.

We can now introduce a simpler charge non-conserving model. The majority of particles are neutral; furthermore, the charged walkers tend to be repelled from the charged cluster, while the neutral, polarizable walkers are drawn to it. Hence one can expect that most of the growth will result from the aggregation of neutral particles. Therefore, we neglect the term due to the charged particles in Eq. (3.4). The charge effects are taken into account simply by rescaling $Q(t)$. As discussed above, the likely behavior of $Q(t)$ is unknown, and dependent upon many competing effects. Here we will use the simplest possible rescaling rule: we will assume that $Q(t) = A(t)\bar{\sigma}$, where $A(t)$ the overall area of the cluster and the average charge density $\bar{\sigma}$ is assumed to be constant.

We now have a sufficient set of ingredients for a complete growth model. That is, a given initial shape determines the charge distribution and hence the electric field. The latter then allows a growth increment in time dt to be computed, yielding a new shape. With the new shape one then computes a new charge distribution and field, and so on.

B. Analysis and Simulation

Now we will show that, with the model as stated, a growing island will eventually transform from a compact to an elongated shape. Consider an island of elliptical shape, with principal axes a, b . If we compute the new boundary, using Eq. (3.4), the new shape will not be exactly elliptical; however, the ellipse’s field may still be used as an approximation. It is then obvious that this new ellipse will have greater eccentricity than the original one if

$$\frac{a + G(a, 0)dt}{b + G(0, b)dt} > \frac{a}{b} \quad , \quad (3.6)$$

which (considering only growth from neutral walkers) is equivalent to

$$\frac{G(a, 0)}{G(0, b)} = \exp\left\{\frac{\chi}{2}\left[E^2(0) - E^2(\pi/2)\right]/kT\right\} > a/b \quad . \quad (3.7)$$

The electrostatic field $E(\phi)$ at distance δ from the point $(a \cos \phi, b \sin \phi)$ is given by

$$E^2(\phi) = \frac{Q^2}{2\delta ab}(b^2 \cos^2 \phi + a^2 \sin^2 \phi)^{-1/2} \quad (3.8)$$

After introducing the average charge density $\bar{\sigma} = Q/A$, where $A = \pi ab$ is the total area of the cluster, Eq. (3.7) becomes

$$\exp\left[\frac{\chi\bar{\sigma}^2\pi^2}{2kT\delta}(a-b)\right] > \frac{a}{b} \quad (3.9)$$

It is obvious from this equation that, if at some time during the growth the relationship (3.9) becomes valid, it will remain valid afterwards. Initially, the shape is compact (circular), i.e. $a = b = R$. However, due to the stochastic aspect of the growth there are always small variations in the radius. One can expect that the magnitude of these variations is at least $\sim \delta$, that is $|a - b| \sim \delta$. The transition from the compact to elongated shape occurs when the compact shape becomes unstable with respect to such variations. This happens when R reaches some critical value R_0 , determined by

$$1 + \delta/R_0 = \exp\left(\frac{\chi\bar{\sigma}^2\pi^2}{2kT}\right) \quad (3.10)$$

or

$$R_0 \approx 2\delta kT/\chi\bar{\sigma}^2\pi^2 \quad . \quad (3.11)$$

Now, estimating $\bar{\sigma} \sim \alpha e/\delta_m^2$, $\chi \sim 2 \times 10^{-24} \text{cm}^3$, $\delta_m \approx \delta \sim 10^{-7} \text{cm}$, $\alpha = 10\%$, and $T \approx 300K$, we get the estimate $R_0 \sim 0.2\mu\text{m}$. Although this estimate is very rough, it is encouraging to see that R_0 is smaller (by roughly an order of magnitude) than the size of seahorses observed in the experiments [14,15].

Thus we find an instability of a compact, circular cluster to an elliptical form, when the compact cluster exceeds a critical size. We have studied the growth of ellipses numerically, and verified that the elongation decays for $R < R_0$; while for $R > R_0$ the elongation persists and grows well beyond the linearized form, and in fact is amplified (and ‘pinched’) by the resulting growth, to give two arms. We have also numerically tested instabilities to four arms. Here we find, for the parameters that we have explored, that the two-arm instability is dominant over four-arm instabilities.

It is clear that, for most cases of interest, neither the charge density nor the electric field can be computed analytically. Hence we need to implement our growth model numerically. This can be done as follows. The current boundary of the cluster is represented as a set of vertices $\{\vec{r}_v : v = 0 \dots N_b - 1\}$, connected by line segments. For each vertex we compute the potential energy of a walker near this point $U(\vec{r}_v)$; then a unit normal vector \hat{n}_v , and the displacement vector $\vec{\Delta}_v = \hat{n}_v G(\vec{r}_v)\Delta_t$ are computed (where Δ_t is a time-scaling constant). After all displacements are computed, all vertices are moved to their new positions. The only remaining problem is to compute the field distribution near the boundary.

One can try to deal with this problem by solving straightforwardly Laplace’s equation for the electrostatic potential. However, despite the fact that our problem is 2-dimensional, Laplace’s equation for the electrostatic

potential is still 3-dimensional. Hence, to find the local electrostatic field, one would need to solve this 3D problem for the full space. To take advantage of the lower dimension of the problem, we will use a surface charge method [29–32], which we will outline below.

Given the cluster C , we first compute the 2D charge density $\sigma(x, y)$, and then find the electrostatic field. To find $\sigma(x, y)$, we introduce a grid $\{\vec{D}_i, i = 1, \dots, N_g; \vec{D}_i \in C\}$, forming a square lattice inside the cluster. Each square of this lattice is assigned a charge density σ_i (we will refer to these squares as elements). Now we replace the continuous equation for the electrostatic potential $V(x, y) = \text{constant}$ for all $(x, y) \in C$ by the discrete equation $V(\vec{D}_i) = \text{constant}$, which gives rise to the following set of linear algebraic equations:

$$\sum_{j=0}^{N_g-1} U_{ij}\sigma_j = 1 \quad (3.12)$$

where $i = 0, \dots, N_g - 1$, and the scaling constant on the right-hand side (here set to 1) can be chosen arbitrarily (that is, after the system is solved, we can rescale all the σ_i). U_{ij} is the electrostatic potential which would be induced at the point \vec{D}_i by the square element j , if the latter had a *unit* charge density. Therefore, one can approximate U_{ij} as follows

$$U_{ij} = \frac{A_j}{r_{ij}}, \text{ for } i \neq j \quad (3.13)$$

where A_j is the area of the j -th element, and $r_{ij} = |\vec{D}_j - \vec{D}_i|$. For most purposes the accuracy of this point-charge equation is sufficient, but one can also use more accurate expression for U_{ij} which takes into account a quadrupole correction

$$U_{ij} = \frac{A_j}{r_{ij}} \left(1 + \frac{A_j}{24r_{ij}^2}\right) . \quad (3.14)$$

The expression for the self-induced potential is

$$U_{ii} = 3.525 d \quad (3.15)$$

where d is the element size (i.e. the grid step).

Eq. (3.12) can be solved numerically and then the electric field can be computed. However at this point we face a difficulty. As we have seen earlier, the field intensity E diverges near the edge of the cluster. In addition, the charge density itself diverges near the cluster's boundary. Thus we are trying to find small variations in a diverging quantity, which itself depends on another diverging quantity. We can alleviate this problem by introducing line charges along the boundary. That is, in addition to charged square elements, we will assume that the boundary segments are also charged. This modification can be easily incorporated into Eq. (3.12); one needs only to distinguish between the self-potential U_{ii} for square elements, which is given by Eq. (3.15), and the self-potential U_{ii} for line elements at the cluster's boundary, given by

$$U_{ii} = 2w \ln(5.44w/l_i) \quad (3.16)$$

where w is the segment's width (i.e. border width) and l_i is the length of the segment. The accuracy can be further improved by using the exact field of a uniformly charged rod rather than the point charge field given by Eq. (3.13).

As an even further simplification of the problem, we may use the linear (boundary) elements *only*. The basis for neglecting the interior elements (which are exactly zero in 3D) is the fact that the charge density in 2D is the largest near the boundary, so that charges located close to the boundary give the main contribution to the electric field. This simplification not only reduces the number of elements to consider (and thus speeds the computation), but also makes it easy to compute the electric field intensity: to compute a field at distance δ from element i , one can just use

$$\vec{E}_i = 2\hat{n}_i\sigma_i w/\delta \quad (3.17)$$

The Boltzmann factor for a neutral particle in this field is then given by $\exp(\chi E_i^2/(kT)) = \exp(\gamma\sigma_i'^2)$, where $\gamma = 4\chi w^2\bar{\sigma}^2/(\delta^2 kT)$ is the dimensionless interaction constant, and σ_i' is the dimensionless charge density, determined by Eq. (3.12) and by the rescaling condition $\sum(\sigma_i' l_i)/\sum l_i = 1$.

We find this simplification to be very important, because, when the charge density is modeled by a square grid (even if the grid is very fine), the nonuniformity in the charge density (arising from the finite grid step) causes noticeable (artificial) fluctuations in electric field, which are then *amplified* by the growth of the island. In contrast (as will be seen below), if we locate all the charge on the boundary elements then the discretization does not lead to such artifacts. Of course, this simplification results in a less realistic field, but we believe that the main physical features of the system—the charge redistribution within the cluster, and the resulting branch repulsion and competition—are preserved.

We add one further ingredient to our model, namely, the property (i): branching. The branching instability in growing forms is well known [33–35]; it arises in diffusive problems as a result of competition between surface (incoming) diffusion—which tends to favor new branches—and edge diffusion (along the boundary)—which tends to keep the cluster smooth. Such competition may be expressed in terms of a length scale L_0 ; this is essentially the cluster size, or branch length, at which edge diffusion can no longer maintain the smoothness of the growing form, and new branches form. Our continuum model does not explicitly represent the underlying diffusive processes. Hence we include a branching instability in a simple way as follows. When a branch reaches a size L_0 (or after a certain number of growth steps—which is approximately the same criterion, for the fastest-growing branches) we force it to split exactly at the point of the fastest growth (as determined by the charge distribution)

into 2 branches. This branch splitting is just the simplest implementation of the fingering/tip splitting instability which is present in many growth phenomena [3]. This instability arises near the tips of fast advancing branches; and the faster the growth, the more likely the split to occur [3]. For most diffusive problems one may expect branches to form also away from the fastest-growing tips. We have explored this possibility numerically, and find in fact that, if we introduce such branches away from the tips, they do not grow—due to the severe competition present in our model. Hence, in the following, we only describe cases where noise is introduced near the tips of the fastest-growing branches.

Obviously, the model described thus far lacks any source of noise (apart from some tiny numerical noise, which is always inevitably present). This means (among other things) that all symmetries present in the initial shape of the cluster will be preserved during the growth. To explore the possibility of chiral symmetry breaking, then, we need to add some (very small) noise into the system—noise which breaks 2D inversion symmetry.

Based on the considerations above, our typical starting condition for numerical studies is an ellipse, with some very small defects added to represent noise. As mentioned above, the cases of interest, in which the defects induce further branching, occur when the noise is added near the tips—ie, near the long axis of the ellipse. As one test of the sensitivity of the model to *chiral* noise, we have used as a starting form an ellipse with 2 tiny defects, which are small dents placed near (but not at) the tips of the ellipse, along the long axis. The right dent is placed slightly above the x axis, and the left dent slightly below. Thus these defects break 2D inversion symmetry. Fig. 3 shows the results after several generations of branching. We note that the original defects are so tiny that they are almost invisible in Fig. 3; however the original tiny chirality has been increased hugely by the resulting growth. We also see that Fig. 3 bears an obvious resemblance to the experimentally observed “seahorses”. In fact, it has essentially the same geometric properties as a typical experimental seahorse: 1) only 2 main arms; 2) these main arms are curved; 3) the curvature is correlated (that is, the two branches curve in opposite directions); 4) the outer edge of each main arm is covered by “fins” (small dead branches).

It is important to test that such dramatic effects are actually implied by the dynamics of the model, rather than artifactual (ie, resulting from some defects in the implementation of the model). In fact, it is possible to “discover” a chiral symmetry breaking in the present model arising simply from the fact that a certain ordering of points along the boundary (clockwise or counter-clockwise) is present in the numerical algorithm. Such an ordering can break the left/right symmetry of the numerical growth results unless sufficient care is exercised. We have discovered and removed such artifacts in our own algorithm. A good test is then a numerical simulation in which the starting shape is an ellipse with 2 defects

which *do not* break the symmetry (ie, the defects are located precisely at the tips of the ellipse). The result of such a test is presented in Fig. 4: the original symmetry is retained during subsequent growth. Hence we are confident that our numerical studies are free of any *artifactual* chiral symmetry breaking.

Now let us consider in more detail how the observed curvature arises. Fig. 5 gives a more detailed picture of the growth and branching processes at one end of the island. After the first split (Fig. 5a), the new branches compete for further growth (as determined by the electric field), and one of the new branches “dies” [ie, practically stops growing (Fig. 5b)]. The winning branch eventually reaches the critical length and then splits again (Fig. 5c). Let us consider what happens when this branch splits in some detail. First, we note that the new branches “feel” one another. The electrostatic repulsion will cause the charges to redistribute, so that the points of fastest growth will no longer coincide with tips of the new branches. Instead, the fastest growth will occur at points of maximal local charge density (hence maximal $|\vec{E}|^2$), which are farther away from each other than tips of the branches. This will force the branches to curve away from one another. If the split is originally symmetric, then the result of the competition between the new branches will be determined by the influence of all the other (already dead) branches. In particular, the main body (being closer to the lower branch) favors the upper new branch (branch 3), while the previous branch (branch 2) favors the lower new branch (branch 4). Branch 2 is smaller than the main body, but the main body is further away. Hence, if the parameter values are right (in particular, if the distance between splitting points is small enough, and dead branches are large enough), then the nearby dead branch has a dominant influence, and so branch 4 will win the competition. Then, due to the exponential difference in the growth rate, branch 2 will stop growing. If this sequence is then repeated, the main arm curves further to the right at each branching.

A similar process happens on the opposite end of the cluster. Hence we see how the present model leads to two main arms, each of which may be rather strongly curved. An ‘S’ shape (rather than a ‘C’ or a ‘3’ shape) results if the direction of curvature is the same for both main arms; that is, the two arms must show a *correlation* in curvature. This implies that one end of the growing body is significantly affected by the form of the distant end. We believe that this point is important: curvature itself, such as shown in Fig. 5, may be ascribed to relatively *local* effects. However the correlation giving rise to consistent ‘S’ shapes appears to *require* some form of long-ranged communication between the parts of the growing island. It is interesting to note here that, in a small minority of the experimentally observed islands, there are two arms whose curvature is in opposing directions—giving a ‘3’ form rather than an ‘S’ [16].

This correlation is not tested by our Fig. 3, since it is

built into the starting condition. We demonstrate that such a correlation does occur in the present model in Fig. 6. Here the starting condition is an ellipse with one (right) defect off axis (to break the symmetry), but the other one precisely on axis. We see that the growth dynamics not only causes the right arm of the cluster to curve downwards, but also determines the outcome of the competition at the other end of the island. It is clear from the figure that the growth at this end is initially symmetric; yet subsequently, the upper arm dominates, purely due to influence from the other end of the cluster. We see that ‘clockwise’ growth at one end has sufficient influence to force clockwise growth at the other. Thus we find that dominance and curvature *are* correlated between the two main arms, leading to strong chirality of the overall cluster.

We have also examined the case that both defects are on the same side of the main axis. Here too we find that the two branches, while initially curving as expected from the local bias, after some growth ‘feel’ one another and so are repelled. We believe however that this starting condition is less realistic than those in Figs. 3 and 6, because the noise we introduce into our continuum model does not represent truly microscopic noise, but rather that noise that may be expected to grow beyond the microscopic scale. This is because the continuum model itself is not a truly microscopic model. Below (section IV) we will give evidence from our microscopic Monte Carlo studies that this continuum model does indeed capture important features of the large-scale behavior of a microscopic model with noise—in particular, the two-arm instability, and the repulsion between these two arms.

It is entirely plausible that a “non-local” effect such as the correlation of curvature shown in Fig. 6 is more fragile than the more local effects shown in Fig. 5. This is true experimentally [16]: as noted above, while the large majority of individual experimental clusters form an ‘S’ shape, some do not. Yet it is precisely this kind of long-distance correlation that gives rise to the broken inversion symmetry: in the absence of such correlation, half of the two-armed islands would have a ‘3’ or ‘C’ shape—and these shapes are not 2D chiral.

Finally, we wish to demonstrate in yet another way that the dramatic symmetry breaking shown in Fig. 3 is a genuine outcome of the growth dynamics of our model: that is, the ‘S’ shape is not a *necessary* outcome of the growth model, yet neither does it require fine tuning of the model parameters. Starting with the same initial form as that leading to Fig. 3, we have performed simulations for different values of the two model parameters: L_0 (the branching length), and the electrostatic interaction constant γ . The results are presented in Fig. 7.

A number of conclusions may be drawn from Fig. 7. We see clearly that *branching* is important for obtaining S shapes: in the bottom row of the figure, branching is essentially absent, and the resulting forms amplify the broken symmetry of the initial condition only rather weakly. We also see that charge effects are equally impor-

tant. They are weak in the left-hand column of Fig. 7; and the resulting forms are uninteresting, regardless of the branching length. Finally, we note that, while both of these effects are important—in that they must be present in order that ‘interesting’ growth forms result—fine tuning of the two model parameters is *not* needed: we see clear two-armed ‘S’ shapes over a central region of the parameter space.

In short: Fig. 7—along with the previous figures—demonstrates rather clearly that growth dominated by (electrostatic effects + branching) *can* give rise to spontaneous ‘S’ shapes which strongly break 2D inversion symmetry, and that these forms are *not* simply modeling artifacts arising either from fine tuning or from being built into the model by hand.

We thus assert that our model possesses a genuine *chiral* growth instability; that is, it can drastically amplify any tiny perturbation that breaks the left/right symmetry. Such ‘drastic amplification’ is of course what is meant by the term ‘spontaneous symmetry breaking’—which is also an appropriate description. Hence the kind of pattern-forming behavior studied here falls into the same, quite rare class of behavior as that seen in phyllotaxis [19,20].

IV. MONTE CARLO STUDIES

We have performed a number of MC studies of aggregation under conditions where the aggregate is charged, and there are both charged and neutral walkers. The most obvious obstacle to overcome is the size of the clusters; as mentioned earlier, there are 10^6 – 10^7 particles in a typical experimental cluster. Thus, in order to perform a successful MC simulation of these experiments, one must find a regime where the desired behavior (formation of S-like clusters) is achieved with smaller numbers of particles.

We have explored a number of MC models, involving various combinations among the following choices: charge-conserving or not (as above); following each walker individually, or making (again) a quasiequilibrium assumption for the spatial distribution of walkers; and treating the cluster as insulating or conducting. Our most encouraging results were obtained using the latter choice in each of the above three cases: that is, modeling only the neutral walkers, treated as a quasiequilibrium gas bonding to a conducting cluster. The resulting model is very like our continuum model in many ways—with the important difference that branching is now a part of the model dynamics, rather than being enforced as a premise of the model.

With the above assumptions, the growth rule is as follows. We perform the growth simulation with the underlying 2D space discretized as a triangular lattice. Given a shape of the cluster (ie a set of occupied sites—our starting cluster is typically a single site), we first find all non-

occupied lattice sites adjacent to the cluster. Then, for all sites simultaneously, we compute the non-normalized probability of a new particle joining the cluster at this site according to

$$P_s = A \exp[(\chi E_s^2/2 + K_s E_b)/kT] \quad (4.1)$$

where subscript s numbers sites along the cluster boundary, E_s is the electric field strength at site s , A is a normalization constant (effectively, the time scaling constant), K_s is the number of sites neighboring site s which are already occupied, and E_b is the bond energy. Thus, again we have a two-parameter model. The strength of electrostatic effects is set by the dimensionless χ . The competition of surface and edge diffusion is contained in the bond energy E_b : large E_b tends to keep the cluster smooth, while small E_b allows small irregularities to grow.

Using this MC model, we were able to reproduce some of the features of the seahorse clusters. Specifically, we found a clear two-arm instability for a significant area of the two-dimensional parameter space. We also found some tendency for the arms to curve, with small dead branches on the outer edges of the curves (Fig. 8). However—recognizing now that the particle number N represents in a sense a third dimension to be explored (with our present range of $N \lesssim 2000$)—we did not find a volume of this three-dimensional space in which the curvature appeared consistently. It is however interesting to note that, where curvature did appear, there was an apparent tendency for the curvature of the two arms to be correlated.

As mentioned above, in tests of our continuum model we found that there was a four-arm instability, which however was weaker than the two-arm instability over a range of growth parameters. One can also see this from Fig. 7: for some parameters, one finds four dominant arms, and for others, two. Here we see the same competition in Fig. 8: two arms have grown to dominance, yet there are two others which have not entirely stopped growing. We have also plotted out a two-dimensional ‘map’ of MC growth patterns, depending on the electrostatic parameter χ and the smoothness parameter E_b/kT . We find that this ‘map’ is qualitatively like that shown in Fig. 7: compact shapes for small χ and large E_b/kT (roughly equivalent to small γ and large L_0 in the continuum model); and two, relatively straight, arms for large χ and small E_b/kT . There are also some significant differences between the two maps. One difference is (again) that we find no region [in (χ, E_b) space, at $N \sim 2000$] of consistent curvature of the two arms, giving S shapes. Another is some tendency for three or six arms to appear; this is almost certainly an artifact of the underlying triangular lattice.

Clearly these results support some important aspects of the picture gained from our other, less microscopic models, even as they fail to give ‘seahorse’ forms. The two-arm instability, with the tendency for the two arms

to lie $\approx 180^\circ$ apart, is clear; also the microscopic parameters χ and E_b/kT give qualitatively the same growth behavior as do γ and L_0 in the continuum model. However we have not found consistent S shapes from the MC models that we have explored. We believe that MC simulations with larger N are needed to test these ideas and results further. It is clear that the kind of repeated branching and death shown in Fig. 5 requires a minimal number of microscopic particles in an aggregate before it can appear. Each dead branch which plays an important role in driving the curvature must be formed of some minimum number of particles; and there must be several generations of dead branches—and of course concomitant growth of the entire aggregate—for the curvature to become significant. We believe that our current results are below that threshold in N (assuming that it exists). Our current MC results also show too much dominance from both noise and the underlying lattice. It is clear from Fig. 8 that artifacts from the underlying lattice are not negligible at the small scale of the figure. Also, microscopic noise is still large at this scale, compared to the other physical effects influencing the growth. Both of these effects will become less important at larger N .

V. GROWTH IN AN EXTERNAL ELECTROSTATIC FIELD

The results that we have presented above represent an unusual form of symmetry breaking in the modeling of growth phenomena. While these studies were inspired by the same unusual symmetry breaking seen in the ICB experiments [14–16], it is by no means certain that the mechanisms explored here are in fact responsible for the observed growth patterns. Our ideas have however motivated further growth experiments, to be reported in detail in a separate publication [16]. Here we will briefly describe the idea of the experiments, and the corresponding simulation studies that we have done, using our continuum model.

ICB growth experiments have been performed as in Refs. [14] and [15], with the single change that there is imposed an external electrostatic field in the plane of the films. The motivation is to test whether electrostatic effects are indeed important for the growth forms; and the results [16] say that they are. Qualitatively, the in-plane field tends to give three effects: (a) the curvature of the main arms is reduced by the field, and even eliminated in a sufficiently strong field; (b) growth appears to be predominantly at one of the two main arms; (c) there is a *weak* tendency (which cannot be distinguished with certainty from zero) for the straightened clusters to grow in alignment with the external field.

It is straightforward to include an external electric field in our continuum simulations, by adding another term to the equations (3.12) for the charge densities. A typical result from such a simulation is presented in Fig. 9.

The starting condition is the same as for Fig. 3. We see that the cluster has lost most of its curvature. Also there is some competition between the tendency to curve (which is favored by the starting defects) and the external field (which tends to align the growth along the field direction). The result of this competition is (roughly) a straight branch, growing at an angle to the field. These results show a good qualitative agreement with the experiments: (a) the curvature of the main arms is suppressed; (b) only one arm grows; and (c) there is some weak tendency for growth to follow the direction of external field, and at the same time, some reason to expect the growth to deviate from the orientation of the external field.

VI. CONCLUSIONS

Despite the obvious resemblance between the experimental results and our simulations, many questions need to be answered before one can claim that our model is directly related to the experiment. First, TCNQ crystals are not conducting [36,37]. However they are believed to have a large (about 8) dielectric constant [38]. Obviously, the polarization charge distribution on the surface of a dielectric will be different from the charge distribution on the surface of a conductor; but the larger the dielectric constant, the smaller this difference is. Second, our model relies crucially on the assumption of slow growth (this assumption leads to exponential differences in growth rates). It is not clear how close this assumption is to what really happens in the experiments. Third, there are very large uncertainties regarding the likely behavior of $Q(t)$, the charge on an island as a function of time. Finally, there is one feature in the experimental patterns that can almost certainly not be obtained from our electrostatic mechanism alone, namely, in the experimental seahorses the curvature is strong enough and prolonged enough that the main arms commonly bend back to touch the central body of the island. We speculate that the addition of crystalline anisotropy effects at grain boundaries can yield this kind of behavior.

One might argue that some other kind of long-range force—for example that coming from elastic effects—might produce an S shape. Of course we cannot rule out this possibility. However the physical effects expected from elastic forces are rather different from those explored here, arising from electrostatic effects. Elastic stresses are not concentrated at growing tips, but rather at ‘valleys’ of the solid’s boundary. Also, in our picture the electrostatic effects are important beyond the boundary of the aggregate. Elastic forces can also extend through the substrate, beyond the boundary of a growing island, during epitaxial growth on a crystalline substrate [39]; however such effects seem likely to be much smaller for an amorphous substrate such as that used in the ICB deposition experiments. Finally, it is not clear to us how elastic forces could give the broken symme-

try seen experimentally, nor the strong sensitivity of the growth patterns to an external electric field [16]. We do note however that some *combination* of elastic and electrostatic effects may be needed to give rise to the high degree of ‘bending back’ of the main arms (noted above) seen in the experimental seahorses.

We comment upon our modeling results. It remains to be demonstrated that all of the features reported here (two arms, branching, consistent correlated “deaths” of branches leading to curvature, and correlation between the curvatures of the two main arms) can be seen to occur together in a single model, with none of them being imposed on the model by construction. Our continuum model shows all of these features but the branching itself (which is uncontroversial); and our MC studies have shown hints (or more) of all of these features. We believe that all of our results, considered together, suggest rather strongly that the principal physical idea explored in our various models—trapped electric charge on a growing aggregate, leading to strongly enhanced growth in regions of strong electric field—can indeed lead to all of these features. However the final demonstration of this remains a challenge to future work in theory and modeling.

In summary: we have proposed a novel mechanism for spontaneous chiral symmetry breaking during 2D aggregation. This mechanism does not rely on the presence of microscopic chirality; instead, it results from the existence of a long-ranged electrostatic interaction in the system, due to a trapped charge on the growing aggregate. This interaction leads to a strong competition and repulsion between growing branches, and—as we have shown here—can give rise to a strongly but *spontaneously* broken 2D inversion symmetry. We have explored several different approaches to the simulation of growth in the presence of such an electrostatic interaction: tree models, continuum models, and Monte-Carlo simulations. Especially encouraging results were obtained using the continuum model; simulated growth often led to clusters which possess the same geometrical properties as the experimentally observed “seahorses” [14,15]. The results of our simulations in the presence of an external electric field are also in good qualitative agreement with the experimental results. Further theoretical work, and further experiments, are needed in order to clarify and test the connection between the ideas presented here and the “seahorse” experiments. However, using physical ideas motivated by the growth experiments, we have found a new class of ‘electrostatic growth’ models which spontaneously break 2D inversion symmetry during growth; and we remain convinced that such spontaneous symmetry breaking occurs in the “seahorse” experiments, and so demands a theoretical model which does the same.

Acknowledgments.— GSC thanks Andreas Deutsch for helpful discussions of bacterial aggregation. This work was supported in part by the U.S. Department of Energy through Contract No. DE-AC05-96OR22464 with Lockheed Martin Energy Research Corp. IMS and GSC were supported by the NSF under Grant # DMR-9413057.

-
- [1] T. Vicsek, *Fractal Growth Phenomena* (World Scientific, Singapore, 1992).
- [2] W. Mullins and R. Sekerka, *J. Appl. Phys.* **34**, 323 (1963).
- [3] J. Langer, *Science* **243**, 1150 (1989).
- [4] P. Safman and G. Taylor, *Proc. Roy. Soc. A* **245**, 312 (1958).
- [5] D. Bensimon *et al.*, *Rev. Mod. Phys.* **58**, 977 (1986).
- [6] U. Nakaya, *Snow Crystals* (Harvard University Press, Cambridge, MA, 1954).
- [7] J. Jacques, A. Collet, and S.H. Wilen, *Enantiomers, Racemates, and Resolutions* (John Wiley & Sons, New York, 1981), pp. 5–7.
- [8] For example, Ref. [1] describes over 150 two-dimensional growth forms, yet only one (bacterial) growth form is 2D chiral (Plate 13); and here the chirality was forced by an experimental constraint.
- [9] M. R. Weis and M. McConnell, *Nature* **310**, 47 (1984).
- [10] E. Ben Jacob *et al.*, *Phys. Rev. Lett.* **75**, 2899 (1995).
- [11] Consider, for instance, a large number of microscopic three-dimensional right hands, each constrained to lay palm down on an orienting interface such as a table top. The resulting collection of two-dimensional hands clearly breaks 2D inversion symmetry, at the microscopic level.
- [12] J. Langer, *Physica Scripta* **9**, 119 (1985).
- [13] Y. Pomeau, *Europhysics Letters* **3**, 1201 (1987).
- [14] H. Gao, Z. Xue, Q. Wu, and S. Pang, *J. Mater. Res.* **9**, 2216 (1994).
- [15] H. Gao, Z. Xue, Q. Wu, and S. Pang, *Solid State Comm.* **97**, 579 (1996).
- [16] H.J. Gao, G.S. Canright, S. Pang, I.M. Sandler, Z.Q. Xue, and Z.Y. Zhang, submitted to *Fractal*.
- [17] R. E. Long, R. A. Sparks, and K. N. Trueblood, *Acta Cryst.* **18**, 932 (1965).
- [18] The polycrystals making up the experimental ‘seahorses’ are actually a metastable crystalline form [16]. It seems likely that centrosymmetric molecules such as TCNQ would assemble in nonchiral crystal structures, just as they do in the ground-state crystal. Also, it seems unlikely that a metastable chiral form of TCNQ would survive the addition of a significant fraction of C₆₀ molecules. However we cannot entirely rule out such a possibility.
- [19] R.V. Jean, *Mathematical Approach to Pattern and Form in Plant Growth* (Wiley, New York, 1984).
- [20] S. Douady and Y. Couder, *Phys. Rev. Lett.* **68**, 2098 (1992); *La Recherche* **24**, 26 (1993).
- [21] T.A. Witten and L.M. Sander, *Phys. Rev. Lett.* **47**, 1400 (1981); *Phys. Rev. B* **27**, 5686 (1983).
- [22] T. Vicsek, F. Family, and P. Meakin, *Europhys. Lett.* **12**, 217 (1990).
- [23] R. Ball, *Physica* **140A**, 62 (1986).
- [24] P. Meakin, *Phys. Rev. A* **35**, 2234 (1987).
- [25] P. Meakin, R. Ball, P. Ramanlal, and L. Sander, *Phys. Rev. A* **35**, 5233 (1987).
- [26] G. Canright (unpublished).
- [27] T. Takagi, I. Yamada, M. Kunori, and S. Kobiyama, in *Proc. 2nd Intern. Conf. on Ion Sources* (Österreichische Studien Gesellschaft für Atomenergie, Vienna, 1972), p. 790.
- [28] I. Yamada, *Appl. Surf. Sci.* **43**, 23 (1989).
- [29] Y. Uchikawa, T. Ohye, and K. Gotoh, *Electr. Eng. Jpn* **101**, 8 (1981).
- [30] Y. Kuno and Y. Uchikawa, *IEEE Trans. on Magnetics* **21**, 2523 (1985).
- [31] Y. Kuno *et al.*, *IEEE Trans. on Magnetics* **24**, 295 (1988).
- [32] H. Murata, T. Ohye, and H. Shimoyama, *Proc. SPIE* Vol. 2858, pp. 103–114 (1996).
- [33] J. Villain, A. Pimpinelli, L.H. Tang, and D. Wolf, *J. de Physique I* **2**, 2107 (1992).
- [34] Z.Y. Zhang, X. Chen, and M.G. Lagally, *Phys. Rev. Lett.* **73**, 1829 (1994);
- [35] M.C. Bartelt and J.W. Evans, *Surf. Sci. Lett.* **314**, L829 (1994).
- [36] K. Kojima, A. Maeda, and M. Ieda, *IEEE Trans. on Electrical Insulation* **27**, 629 (1992).
- [37] Y. Osada *et al.*, *J. Appl. Phys.* **64**, 1476 (1988).
- [38] G. Mondio *et al.*, *J. Mater. Res.* **8**, 2627 (1993).
- [39] Q. Xie, A. Madhukar, P. Chen, and N.P. Kobayashi, *Phys. Rev. Lett.* **75**, 2542 (1995).

FIG. 1. The first two steps of a charged tree’s growth. At every step, the tree selects a configuration with the lowest electrostatic energy. For the first step one of the rejected configurations is shown above the transition arrow.

FIG. 2. The growth of a conducting tree. $l_1 = 0.7$, $l_0 = 0.5$ (arbitrary length units); $\theta = 12^\circ$. In this case, growth according to an energy-minimization rule leads to an ‘S’ shape.

FIG. 3. Sixty time steps in the growth of a charged island. The starting condition is an ellipse with two tiny defects, each placed just counterclockwise of the ellipse’s symmetry axis. The tiny symmetry breaking present in these defects is dramatically enhanced by the subsequent growth.

FIG. 4. Growth of an ellipse with 2 tiny *symmetrically* located defects. Such a shape preserves its symmetry during the growth. Hence the symmetry breaking seen in the other figures is not artifactual.

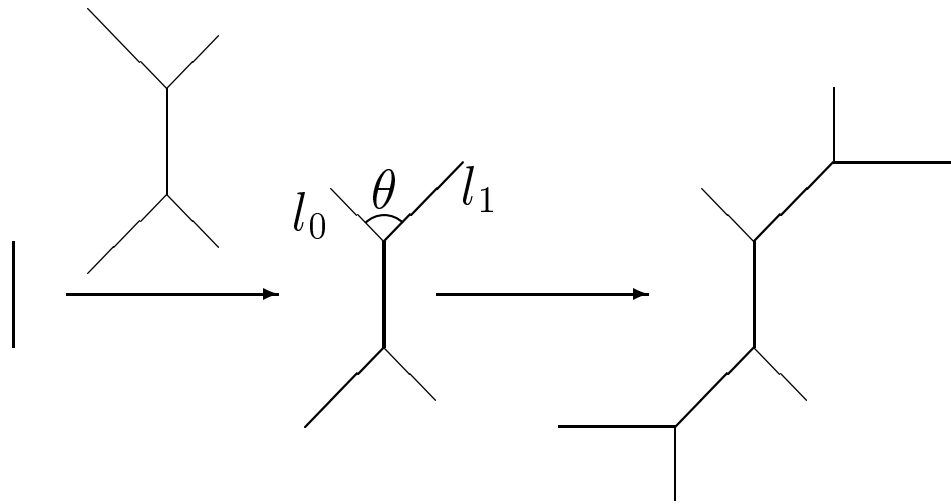
FIG. 5. Early stages in the growth of the right half of Fig. 3, viewed in detail. (a),(b) The broken symmetry in the original (tiny) defect leads to dominance of the lower branch. (c) The growing branch 1 splits again. (d) The nearby “dead” branch 2 inhibits branch 3, so that again the lower branch dominates. In this way the ‘memory’ of the *handedness* (right or left) of the original small defect is maintained and amplified by the subsequent growth.

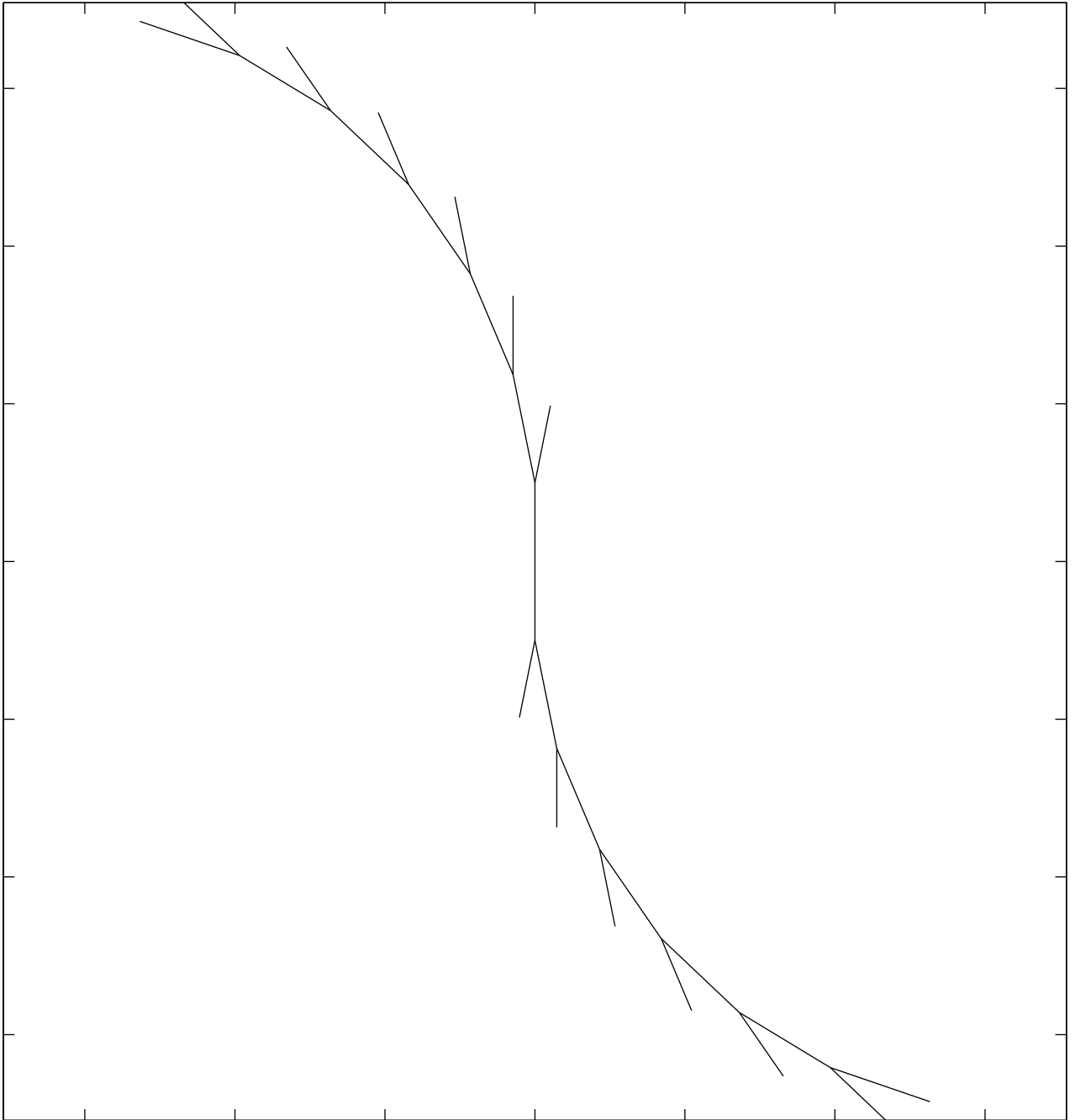
FIG. 6. Growth from an initial shape in which one defect (on the right) is off the symmetry axis, but the other (on the left) is on the symmetry axis. The broken symmetry on the right-hand side still has a large effect on the growth of the left-hand side—in fact, it causes the same (clockwise) branch to dominate there, even though the left-side defect is symmetrically placed.

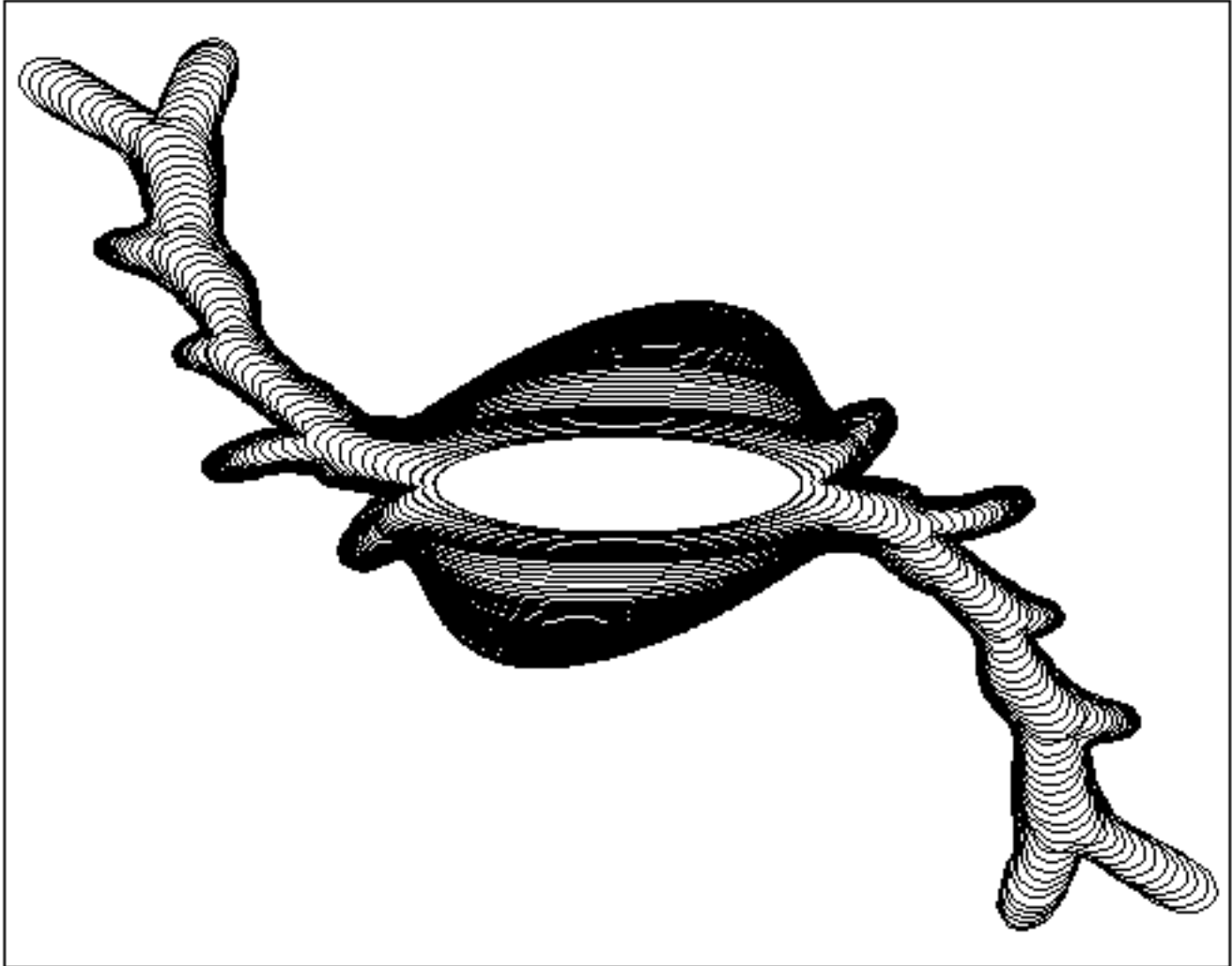
FIG. 7. Growth forms for different values of the branching length L_0 (increasing downwards) and the interaction constant γ (increasing to the right). There is a region of the figure (roughly, the center) in which growth gives ‘S’ forms resembling those seen experimentally. However if the electrostatic effects are too weak (left side) or branching is too infrequent (bottom) then other forms result, displaying little or no chiral symmetry breaking.

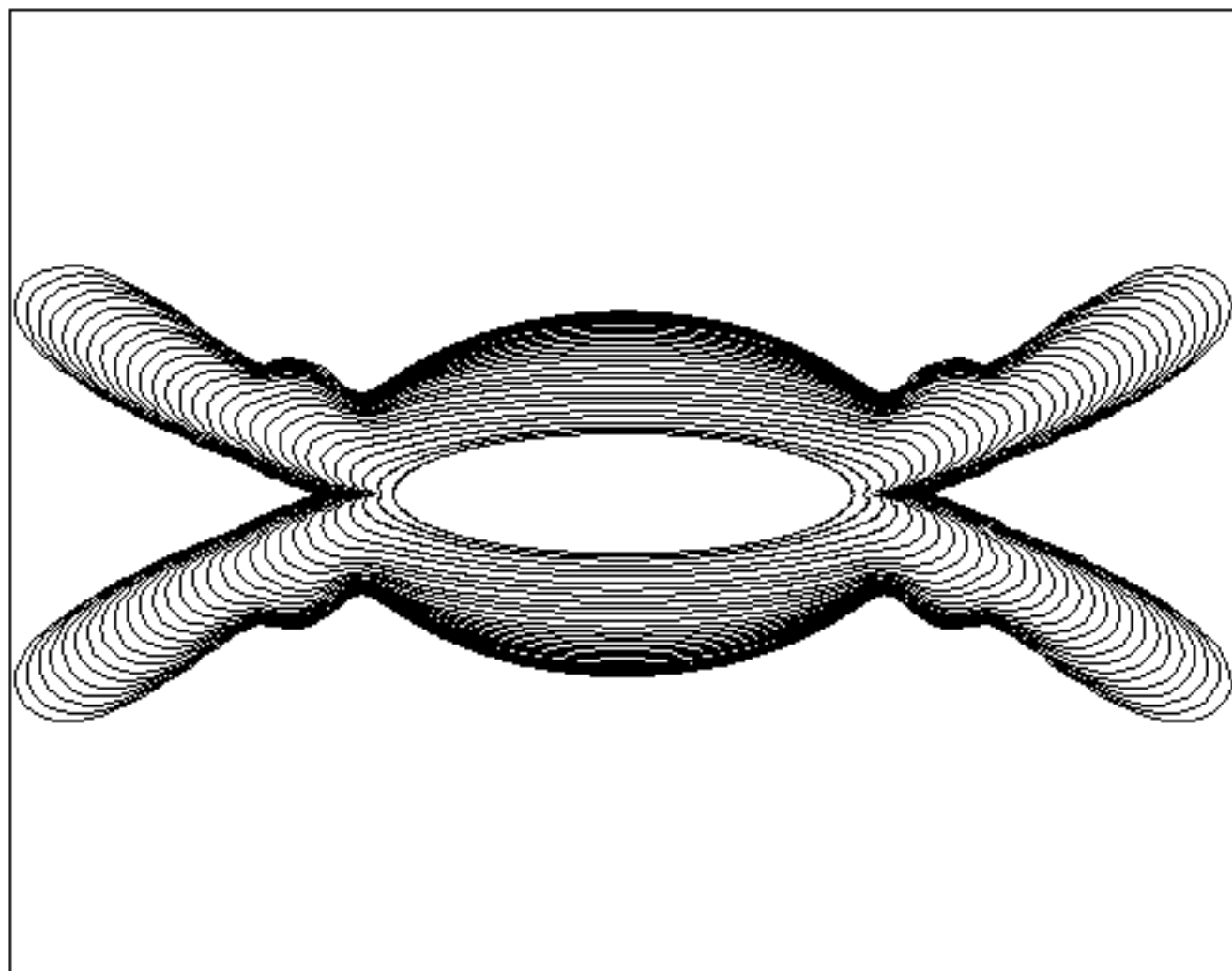
FIG. 8. A 2300-particle cluster grown using a Monte Carlo algorithm on a triangular lattice. The growth rule is described in the text; growth parameters are $\chi = 1.0$ and $E_b/kT = 2.5$. Although this cluster looks promising, we have not obtained such results consistently. It is probably necessary to use larger particle numbers to obtain such forms consistently.

FIG. 9. Growth in the presence of an external electrostatic field, oriented horizontally to the right. Starting conditions and growth rule are otherwise as in Fig. 3.

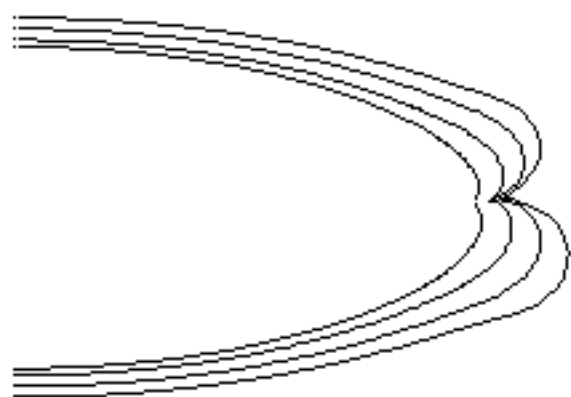




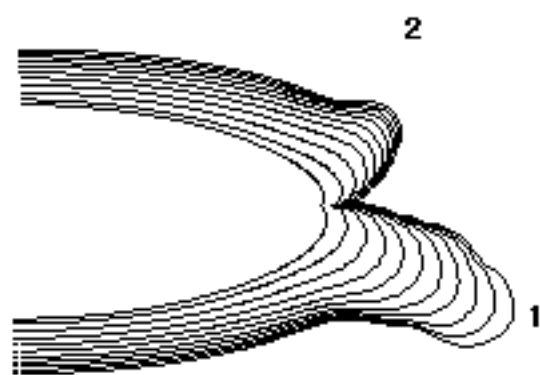




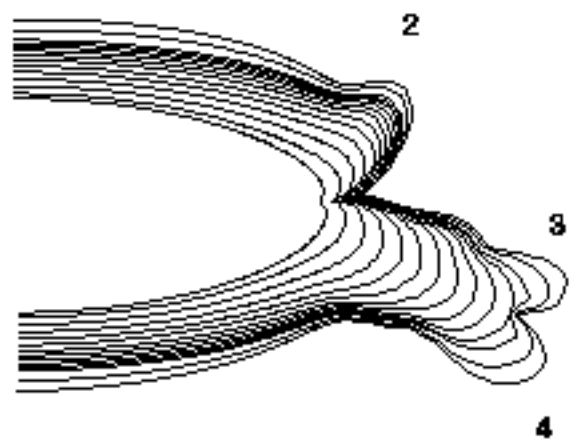
(a)



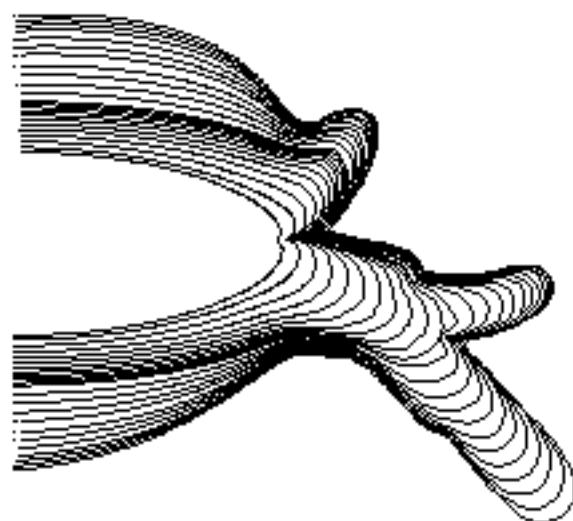
(b)

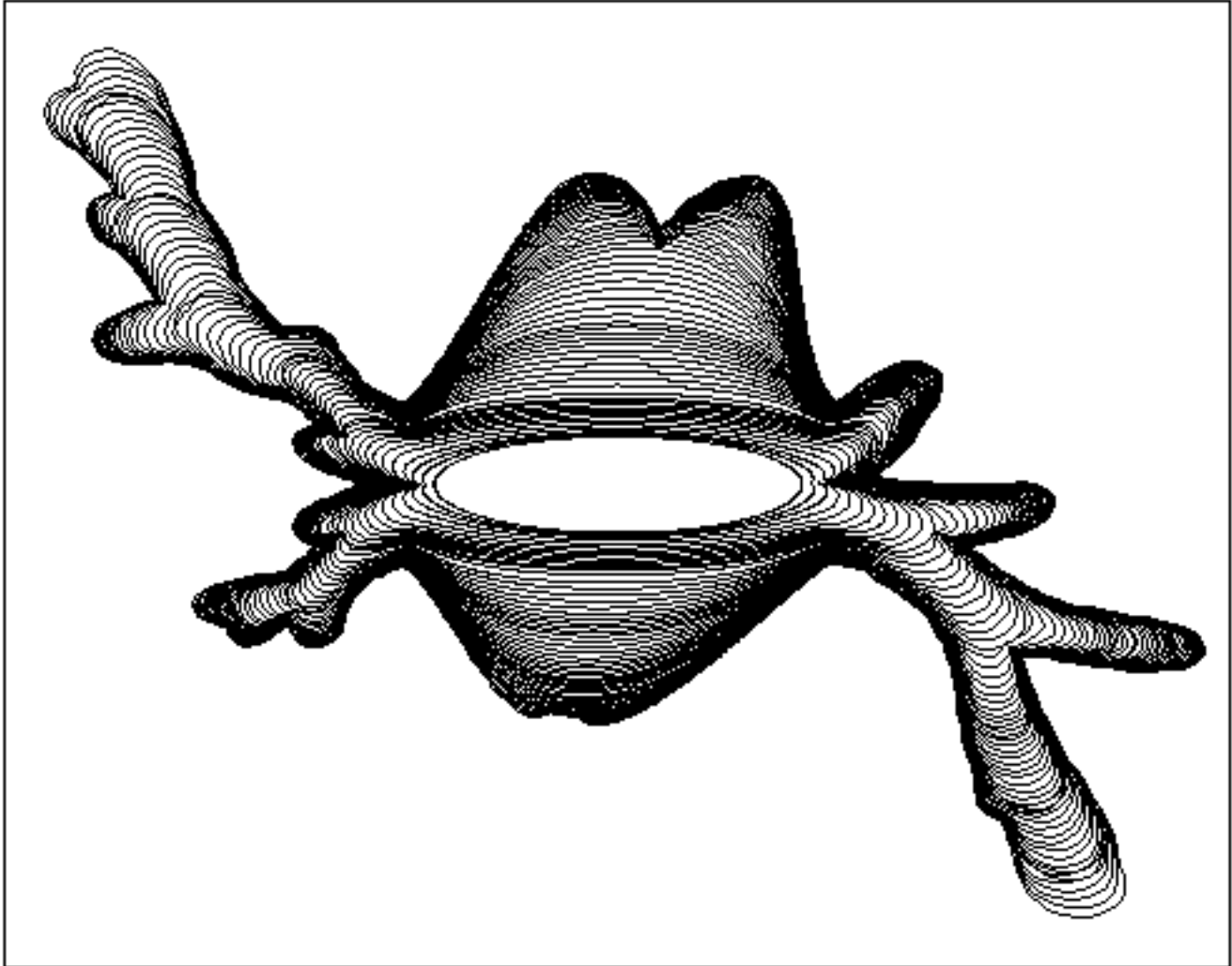


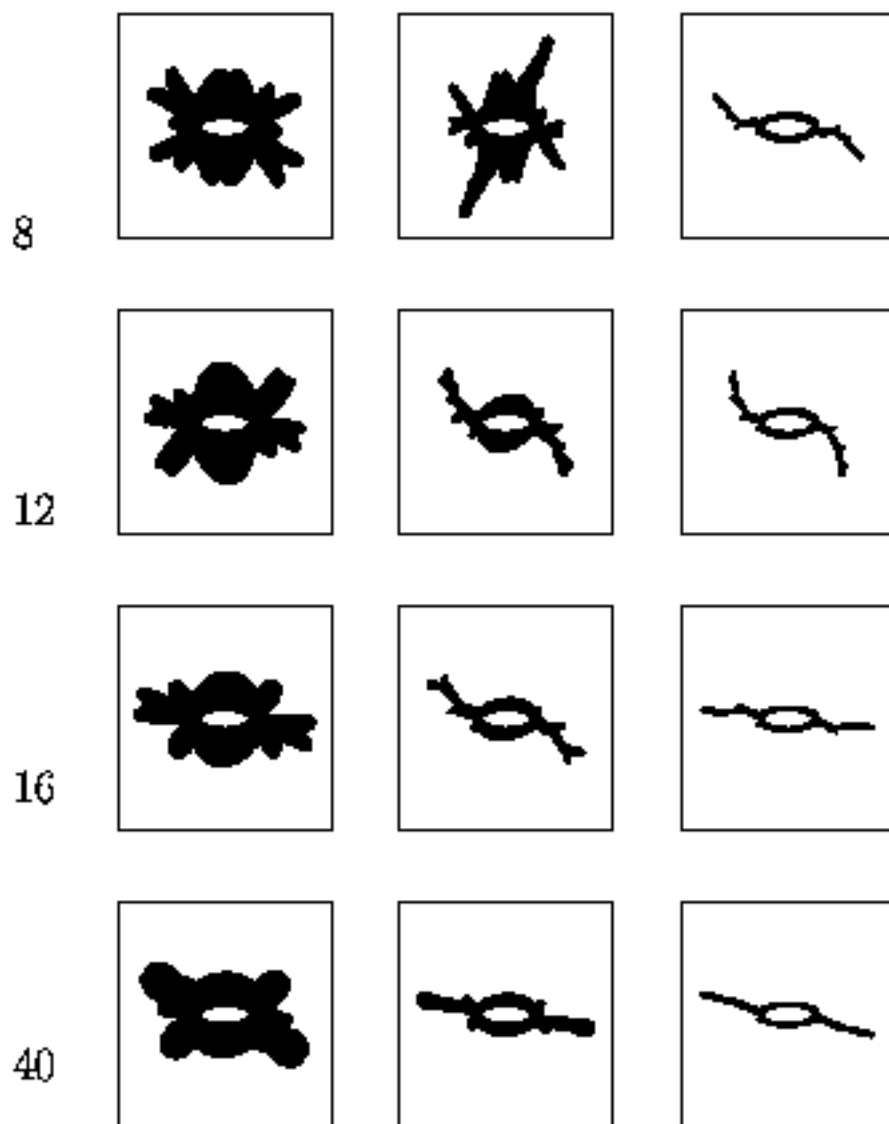
(c)



(d)







$L_0^\dagger \gamma \rightarrow 12$

16

20

